Space Interferometry Mission: Preliminary Error Budgets for Spacecraft Pointing Requirements

Allan Y. Lee†, Jeffrey W. Yu, Peter B. Kahn, and Richard L. Stoller

Jet Propulsion Laboratory, California Institute of Technology

†M.S. 198-235, 4800 Oak Grove Drive, CA 91109-8099. Email: aylee@jpl.nasa.gov. Tel: (818)-354-4097.

Abstract

Preliminary error budgets for the pointing knowledge, control, and stability of the SIM spacecraft are constructed using the specifications of commercial off-the-shelf attitude determination sensors, attitude control actuators, and other spacecraft capabilities that had been demonstrated in past missions. Results obtained indicate that we can meet all the presently known spacecraft pointing requirements. A large number of "children" requirements are generated from this study. Examples are specifications on attitude determination sensors, attitude control actuators, minimum settling time after a rest-to-rest spacecraft slew, etc. Since the SIM spacecraft design is expected to evolve with time, pointing requirements stated in this study are likely to change with it. Hence, error budgets constructed here must be revised to reflect the changing spacecraft design and the addition, deletion, and/or modifications of spacecraft pointing requirements. Results given here represent only the first step.

Table of Contents

1. Introduction
2. Spacecraft pointing requirements
3. SIM attitude control subsystem
4. Component error contributors
   - 4.1 Attitide determination error
   - 4.2 SRU bias
   - 4.3 Inflight calibration residual error
   - 4.4 Thermal distortion of structure
   - 4.5 Slew-induced vibration
   - 4.6 RWA controller error
   - 4.7 RWA-induced vibration
   - 4.8 S/C-solar array control interaction
   - 4.9 Thermal flutter
   - 4.10 Spacecraft-interferometers control interaction
5. Preliminary error budgets
6. Conclusions
7. References
8. Acronyms
9. Acknowledgments
10. About the authors

1. Introduction

In the year 2005, the National Aeronautics and Space Administration (NASA) Space Interferometry Mission (SIM) will send a powerful interferometer into space to operate above the Earth's atmosphere. SIM will yield star positions 250 times more accurately and narrow-field imaging with four times finer resolution than the best currently available techniques. These goals are to be achieved via a technique called optical interferometry. A preliminary "Rainbird Configuration" design of the SIM spacecraft is depicted in Fig. 1.1 (Aaron, 1998).

An interferometer uses two telescopes on a common baseline to collect light from a target star. Because of SIM orientation, the star light wavefront will reach the two telescopes at different times, causing one light path to be shorter than the other. Astrometry determines the angle between the target star and the interferometer baseline. This angle can be found if we can

determine the path-length difference and the baseline length between the two telescopes. To determine the path-length difference, one branch of the two light waves is "delayed" via an active optical delay line before it is being "combined" with the other light wave to form an interference pattern. A bright fringe appears on a detector when the external and internal (that generated by the optical delay line) path-length differences are exactly the same. By making accurate measurements of both the internal path-length difference and the baseline length using a laser metrology system, the location of the star can be determined. For further information on optical interferometry, see Rayman and Shao, 1992.

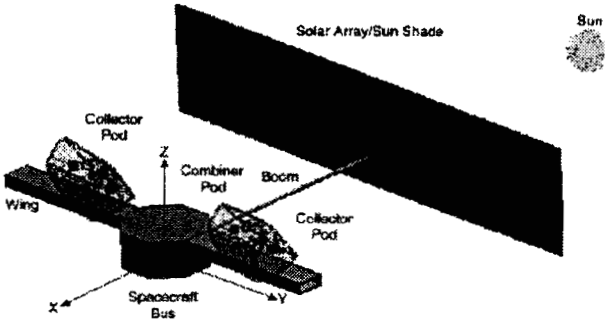

Fig. 1.1 The SIM "rainbird" configuration

Major science goals of the SIM mission include the following. For astrometry in visible light (0.4 to 1.0 μm wavelength), SIM will measure star positions to an overall mission accuracy of better than 4 $\mu\widehat{sec}$ over wide angles (15° FOV), and to 0.26 $\mu\widehat{sec}$ over narrow angles (1° FOV). For imaging very small objects, or selected regions of larger objects, the SIM's imaging resolution goal is 10 mas (1 mas $=10^{-3}\widehat{sec}$). In support of the Terrestrial Planet Finder program, SIM will demonstrate a technique called interferometric nulling. Here, SIM goal is to be able to reveal the properties of protoplanetary disks to within a few AU from the star, perhaps revealing structures in the disk attributable to a planetary system.

2. Spacecraft Pointing Requirements

In this paper, the spacecraft on-board pointing knowledge error is defined to be the magnitude of the error vector between the actual pointing vector and the pointing vector estimated by the on-board attitude estimator. Similarly, the pointing control error is the magnitude of the error vector between the desired and actual S/C pointing vectors. See Fig. 2.1.

A so-called "peak-to-peak" pointing stability metric is commonly used to specify the level of motion stability of a given S/C body axis or the line-of-sight (LOS) of an on-board instrument. One drawback of this stability metric is that it uses only the two extrema points in the time history of the pointing vector that fall within a time window of interest. Another pointing stability metric that has been used in past missions is the Root-Mean-Squares (RMS) pointing stability metric (S_{rms}). If B(f), in $\widehat{sec}/\sqrt{Hz}$, denotes the frequency spectrum of the LOS motion, then:

$$S_{rms} = \sqrt{\{ \int_0^\infty B^2(f)df \}}.$$

where f = frequency. This is a straight-forward way to measure motion stability. However, the degree to which disturbances at different frequencies contributed to jitters is also a function of the time window of interest, T, which is not considered in defining S_{rms}. In this study, a "weighted" RMS pointing stability metric, S_{wrms}, first introduced by Lucke, Sirlin, and San Martin (1992), is adopted. In the frequency domain, it is defined as follows:

$$S_{wrms} = \sqrt{\{ \int_0^\infty B^2(f)W_d(C)df \}}.$$

where $C = 2\pi fT$, and $W_d(C)=1-2(1-\cos C)/C^2$.

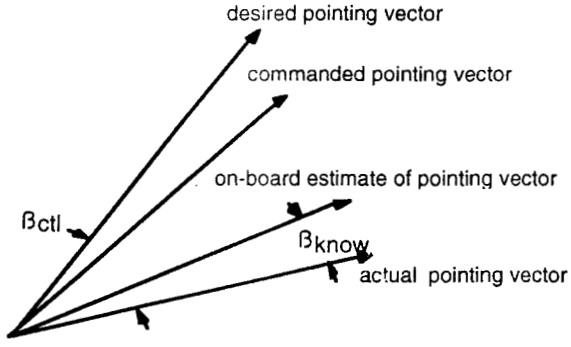

βknow = on-board pointing knowledge error

βctl = pointing control error

Fig 2.1 Spacecraft pointing vectors

Three coordinate frames are first defined in order to better describe various SIM spacecraft (S/C) pointing requirements. The spacecraft mechanical frame C^{MECH} is depicted in Fig. 1.1. Nominally, the X-axis of the C^{MECH} frame is parallel to the nominal direction of the solar array boom. Its Y-axis is parallel to the common baseline of the interferometers, and the Z-axis completes a right-handed XYZ coordinate system. The origin of the C^{MECH} frame is at the center of the separation plane between the launch vehicle and the spacecraft, and the positive directions of the axes are depicted in Fig. 1.1.

The Attitude Control Subsystem (ACS) frame is denoted by C^{ACS}. The inertial attitudes of the three axes

of the C^{ACS} frame are to be estimated by an on-board attitude estimator, using measurements from both the Inertial Reference Units (IRUs) and Stellar Reference Units (SRUs). It will be shown in the following that the spacecraft pointing requirements about both the X and Z axes of the C^{MECH} frame are significantly more stringent than those for the Y axis. As such, the boresight axis of the SRU should be aligned with the Y-axis of the C^{MECH} frame. The other two axes of the C^{ACS} frame are as depicted in Fig. 2.1.

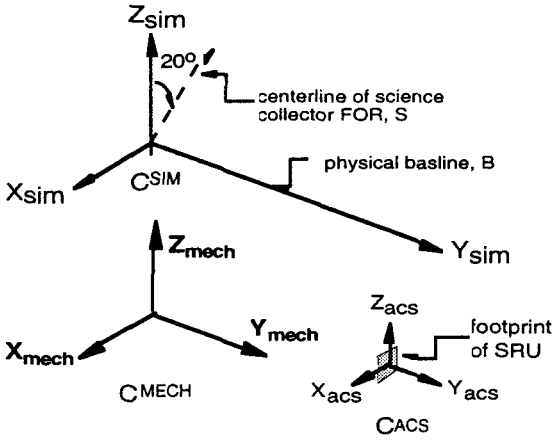

Fig. 2.1 SIM coordinate frames

The coordinate frame with respect to which the spacecraft pointing requirements are to be specified is the SIM reference coordinate frame, C^{SIM}. The common baseline (B) shared by the science/guide interferometers, called "physical baseline", is the Y-axis of the C^{SIM} frame. With reference to Fig. 2.1, let S denotes the centerline vector of the science collector mirror field of regard (nominally, it lies within the +YZ plane of C^{MECH} frame, and is 20° away from the Z-axis). The X-axis of the C^{SIM} frame is parallel to the cross product of the B and S vectors, and the Z-axis of C^{SIM} frame completes a right-handed XYZ coordinate system. The vertex of the left corner cube (the one with a negative Y-axis coordinate in the C^{MECH} frame) is designated the origin of the SIM reference frame.

SIM spacecraft pointing requirements consist of the following: (1) on-board pointing knowledge requirements of 20 $\widehat{\text{sec}}$, 3σ per X and Z axes, and 120 $\widehat{\text{sec}}$, 3σ per Y axis; (2) pointing control requirements of 30 $\widehat{\text{sec}}$, 3σ per X and Z axes, and 120 $\widehat{\text{sec}}$, 3σ per Y axis; and (3) 0.4 mas over a 10 msec time window, 1σ per X and Z axes (and none about the Y axis). Drivers behind these spacecraft pointing requirements are explained as follow.

The S/C on-board attitude knowledge requirements are driven by the need to successfully complete a guide star fringe acquisition within a prescribed time duration. A S/C attitude knowledge error of about 20 $\widehat{\text{sec}}$ corresponds to about 1 mm (3σ) in knowledge uncertainty in the central fringe position (20 $\widehat{\text{sec}}$×10 m ≈ 1 mm). The number of fringe search steps, each of 10 μm, that are required to complete a ±4σ search is: 4×2×(1/3 mm)/10 μm ≈ 267 steps (Chu, 1998). With an integration time of 10 msec for each search step, the worst-case total integration time is 2.67 s. Add to that the stepping time, the estimated time to complete a fringe acquisition is on the order of 4-5 s. which is acceptable.

The S/C pointing control requirements are driven by the need to ascertain that a selected guide star falls within the FOV of the coarse acquisition camera of the guide interferometer when it is commanded to point at that star. In the current SIM design, the FOV of the acquisition camera is 10 $\widehat{\text{min}}$ (Yu, 1998). The 30-$\widehat{\text{sec}}$ S/C pointing control requirement represents a small fraction of that FOV.

The spacecraft pointing stability requirement is driven by the need to maintain a high level of optical pathlength stability during every 10-msec integration time steps during the fringe acquisition process. Good pathlength stability leads to high signal-to-noise on the guide fringes, positively enabling fringe detection. An estimate of an acceptable level of pathlength stability is about 20×10^{-9} m (1σ) (Yu, 1998 and Laskin, 1998). Hence, the pointing stability of the spacecraft , about both the X and Z axes of the C^{SIM} frame, is 20×10^{-9} m/10 m ≈ 0.4 mas (1σ per X and Z axes).

3. SIM Attitude Control Subsystem

The stringent spacecraft pointing requirements described above are to be achieved via a carefully designed Attitude Control Subsystem (ACS) of the SIM spacecraft. Spacecraft's three-axis attitude is estimated using measurements from both the IRUs and the SRUs. To this end, the identities of stars captured by SRU frames are first determined by a star identification algorithm. The inertial attitudes of these identified stars, given in an on-board star catalog, are then used to determine the inertial attitudes of the SRU axes. Between SRU frames, the estimated S/C attitudes are propagated using the IRU measurements. Via periodic inflight calibrations between the SRU's axes (ACS frame) and other body-fixed vectors of interest (e.g., the radio frequency boresight of the Gain Antenna (HGA), axes of the SIM reference frame, etc.), the inertial attitudes of these vectors are estimated.

Three Reaction Wheel Assemblies (RWAs) are used to control the S/C basebody. A fourth RWA is to

be provided as a backup. The RWAs are also used to slew the S/C from one commanded attitude to another. With an Earth-trailing orbit, only solar radiation imparts a significant environmental disturbance torque on the SIM spacecraft. The resultant angular momenta accumulated on these RWAs must then be unloaded using hydrazine thrusters periodically.

The spacecraft ACS also responds to ground-commanded pointing of both the solar array/sun shield (SA/SS) and the HGA. With reference to Fig. 1.1, the SA/SS is attached to the spacecraft basebody via a solar array boom. The relative orientation of the boom with respect to the basebody is to be controlled via a two degrees-of-freedom (dof) solar array drive mechanism (SADM). The attitude control subsystem also performs other engineering functions such as to detumble the S/C after the spacecraft-launch vehicle separation, and to maintain a safe-hold attitude in response to safing requests.

4. Component Error Contributors

4.1 Attitude determination error

The ACS attitude estimator (ATE) is basically a Kalman-Bucy filter that uses, optimally, measurements from a SRU and a set of IRUs. Inertial attitude updates are given by the SRU at intervals of ΔT seconds. In between these star measurement updates, the S/C attitude estimates are propagated using the IRU measurements. See Fig. 4.1.

The performance of the ATE can be estimated using an error covariance analysis. It provides an estimate of the ATE error due to both the rate white noise (angle random walk) and bias instability of the IRU, as well as the Noise Equivalent Angle (NEA) of the SRU.

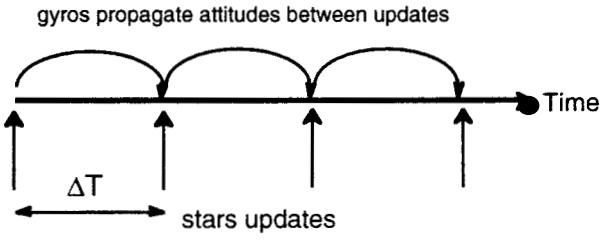

Fig. 4.1 Propagation of the estimated spacecraft attitude

When the S/C is quiescent, the attitude estimator error vector $\vec{e} = [e_x\ e_y\ e_z\ ]^T$ and the IRU bias vector $\vec{b} = [b_x\ b_y\ b_z\ ]^T$ are governed by the following equation: $\vec{x}_k = \Phi_{k-1}\ \vec{x}_{k-1} + \vec{w}_{k-1}$. Here, $\vec{x} = [\vec{e}^T\ \vec{b}^T]^T$ is the state vector of the ATE, and $\vec{w}$ is a zero-mean, white sequence with covariance Q_k. Q_k is given by $\Delta T \times [N_1 \cdot I_3\ 0_3;\ 0_3\ N_2 \cdot I_3]$, where ΔT is the time duration between star measurement updates, and N_1 and N_2 denote the power spectral densities of the IRU rate white noise and bias instability, respectively. The state transition matrix Φ_{k-1} is a constant 6×6 matrix that is approximated by $I_6 + \Delta T \times [0_3\ -I_3;\ 0_3\ 0_3]$.

The measurement equation is given by: $\vec{Z}_k = H_k\ \vec{x}_k + \vec{v}_k$, where $\vec{Z}$ is a 3×1 star measurement vector, H is a constant measurement matrix given by $[I_3\ 0_3]$, and $\vec{v}$ is a vector of zero-mean random noise with covariance R_k (due to the SRU's NEA). The propagation of the error covariance matrix of $\vec{x}$ is governed by the following set of equations:

$$P_k(-) = \Phi_{k-1}\ P_{k-1}(+)\ \Phi^T_{k-1} + Q_{k-1}$$

$$P_k(+) = [I_6 - K_k\ H_k]\ P_k(-)$$

$$K_k = P_k(-)\ H^T_k\ \{\ H_k\ P_k(-)\ H^T_k + R_k\ \}^{-1}$$

where $P_k(-)$ and $P_k(+)$ denote the error covariance matrices of the state vector computed immediately before and after the k^{th} star measurement update, and K_k denotes the Kalman-Bucy gain. Using these equations, we can compute the time propagation of the ATE errors on the three S/C axes. The attitude determination errors given in the following error budget tables (see Section 5) were computed using the following set of sensor specifications: $\Delta T = 0.5$ seconds, $N_1 = 10^{-8}$ deg^2/hr, $N_2 = 0.6 \cdot 10^{-3}$ deg^2/hr^3, and NEAs of SRU are 1.5 and 25 (twist) $\widehat{sec}$, 3σ per axis.

Sensor noise with significant frequency content within the control bandwidth looks like valid "command" to the control loop. The controller commands torque's in order to cause the S/C attitude to follow these erroneous "commands." This results in undesired S/C motion. This effect usually accounts for one of the largest component of S/C pointing instability.

To estimate the impact of both the SRU and IRU noise on the spacecraft pointing stability, we first derive the transfer functions from these sensor noise to the attitude estimator errors using the error propagation equations given above. The power spectra of the spacecraft attitude and rate errors could then be estimated. They are subsequently used in Section 4.6 to estimate their impact on the spacecraft pointing stability.

4.2 SRU bias

The SRU's NEA captures only effects due to photon noise, stray light noise, dark current noise, and readout noise. It does not capture SRU centroiding error, optical distortion, PSF distortion, focal length scale error, and chromaticity. These bias errors account for the difference between the total measurement error of the SRU and its NEA. In this study, the total measurement errors of the SRU are 3.4 and 53 (twist) $\widehat{sec}$, 3σ per

axis.

4.3 Inflight calibration residual errors

The inertial attitudes of the ACS axes are estimated by the ACS's ATE. However, the pointing knowledge, control, and stability requirements are levied not with respect to the ACS frame but rather with respect to the SIM reference frame. As such, the misalignments between these two coordinate frames, which vary from time to time, must be determined via periodic inflight calibrations. Residual knowledge error between these two frames, after an inflight calibration, is another error source that must be accounted for in the error budgets.

In a typical inflight calibration, the "guide" interferometers are commanded to point in the direction of a pre-selected star field. The inertial attitude of the SIM reference frame could then be derived using the inertial attitudes of the captured guide stars provided by the star catalog. The inertial attitude of the ACS frame at the time when the guide stars are captured is available via the time-tagged telemetry data of the ATE. Using these attitude estimates, the misalignment angles between the ACS and SIM coordinate frames could be determined. In general, the attitude estimation errors associated with the guide interferometers are significantly better than those determined by the ATE. Hence, the residual error after an inflight calibration is approximated by the ATE error.

Before the first inflight calibration, pointing of the guide/science interferometers will be affected by structural misalignments between the ACS and SIM frames. The estimated value of the overall structural misalignment is on the order of 0.5-1° per axis (Lee, 1997). With an uncalibrated S/C pointing knowledge error this big, both angle tracking and fringe acquisition of guide stars become difficult. To overcome this problem, we might have to use the coarse acquisition camera of the guide interferometers to perform a spiral (or a mosaic) search around the expected locations of the guide stars. Also, the fringe acquisition time associated with the initial operations of the guide interferometers will be significantly longer than the norm.

4.4 Thermal distortions between inflight calibrations

In between inflight calibrations, thermal distortions of both the SRU mounting surface and the precision structure (upon which both the SRU and the guide interferometers are mounted) generate additional pointing knowledge uncertainties that are not accounted for by the last inflight calibration. The SRU thermal distortion is controlled by imposing thermal stability requirement on the SRU itself. In this study, the per-axis thermal stability of the SRU is ≤4 sec (3σ) over any 30-day period. Implicit in this requirement is the need to perform an ACS-to-SIM calibration every 30 days.

Thermal distortion of the precision structure could be estimated as follows. Let α be the equivalent coefficient of thermal expansion of the precision structure material, $\Delta T/\Delta h$ be the temperature gradient across the surfaces of the structure , and L is a characteristic dimension of the structure. Accordingly, the thermal distortion of the structure is given by: $2\beta_{thermal} = L/R = L \cdot \alpha \cdot \Delta T/\Delta h$, where R is the radius of curvature of the distorted structure (cf. Fig. 4.2). To control $\beta_{thermal}$, we impose bounds on both α and the maximum allowable temperature excursion of the precision structure ΔT. In this study, we use $\alpha = 0.2$ ppm per °C, and the precision structure is to be thermally controlled so that its temperature vary within ±2 °C throughout the five year mission life time. One sec is allocated in the error budgets to account for these thermal distortions.

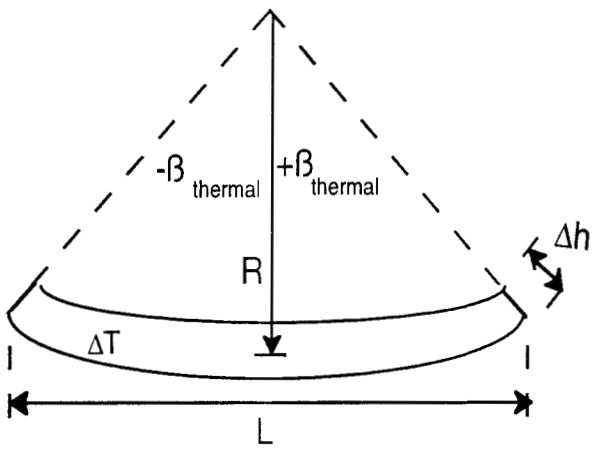

Fig. 4.2 Thermal distortion of the SIM structure

4.5 Slew-induced structural vibrations

When a non-rigid S/C is slewed from one inertial attitude to another, residual structural vibrations after the completion of the slew need not be small. The order of magnitude of these residual vibrations is related to the natural frequencies and damping ratios of the major structural modes, the magnitude of angular acceleration used in slewing the S/C, and the elapsed time between the end of the slew and the time at which science observations is to begin (called settling time, T_s).

In Fig. 4.3, the SIM spacecraft is modeled by two rigid bodies connected by a spring and damper combination. One "rigid" body represents the precision structure while the second represents the solar array/sun shield (SA/SS).

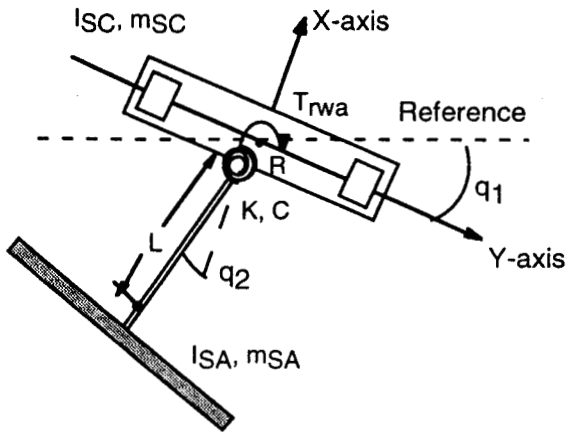

Fig. 4.3 A simplified two-dof SIM model

The equations of motion of this spacecraft model are:

$$[I_{SC}+I_{SA}+m_{SA}(R+L)^2]\,\ddot{q}_1+[I_{SA}+m_{SA}(R+L)L]\,\ddot{q}_2 = T_{RWA}.$$

$$[I_{SA}+m_{SA}(R+L)L]\,\ddot{q}_1+[I_{SA}+m_{SA}L^2]\,\ddot{q}_2 = -K\,q_2 - C\,\dot{q}_2$$

Here, I_{SC} is the moment of inertia of the spacecraft basebody, and I_{SA} is the moment of inertia of the SA/SS (relative to its own center of mass). The angle q_1 is the angular displacement of the basebody with respect to an inertial reference, and the angle q_2 is the displacement of the SA/SS with respect to the basebody. T_{RWA} is the torque exerted on the basebody by the RWAs, and K and C are the spring stiffness and damping rate of the solar array boom. Dimensions R and L are defined in Fig. 4.3. As expected, K and C are related to the natural frequency and damping ratio of the first flexible mode of the structure: $K = \Omega^2\Delta$, and $C = 2\Omega\beta\Delta$, where $\Delta = m_{SA}[I_{SC}L^2+I_{SA}R^2]+[I_{SC}+I_{SA}+m_{SA}(R+L)^2]$. Using these formulae, K and C could be selected to achieve a structural vibration mode with a 1-Hz frequency and a 1% damping ratio.

After a rest-to-rest slew, the residual rate and displacement of the spacecraft basebody are bounded by the following relations:

$$|\text{residual rate}| \le \alpha_{slew} \cdot Q \cdot e^{-\beta\Omega T_s} \cdot \Omega^{-1} \text{ [rad/s]},$$

$$|\text{residual angle}| \le \alpha_{slew} \cdot Q \cdot e^{-\beta\Omega T_s} \cdot \Omega^{-2} \text{ [rad]}.$$

Here, α_{slew} is the angular acceleration used in slewing the spacecraft, T_s is the settling time, and $Q = [I_{SA}+m_{SA}L(R+L)]^2+[m_{SA}(I_{SC}L^2+I_{SA}R^2)]$. Estimated inertia properties of the SIM spacecraft are: m_{SA} = 400 kg, I_{SC} = 36,400 kg-m² (Z-axis), I_{SA} = 5760 kg-m² (Z-axis), R = 1.5 m, and L = 5.9 m. Given $\Omega = 2\pi$ rad/s (1 Hz), β = 1%, $\alpha_{slew} = 5.24\cdot10^{-6}$ rad/s², and T_s = 1 minute, the magnitudes of the residual rate and angle after a rest-to-rest spacecraft slew could be estimated. Using the estimated residual rate, the pointing stability of the spacecraft over a time window of 10 msec could also be estimated.

4.6 RWA controller error

Pointing control of the SIM basebody is to be done using a set of three Reaction Wheel Assemblies (RWAs). A fourth RWA is to be provided as a backup. A representative RWA attitude control loop (Macala, 1994) is depicted in Fig. 4.4.

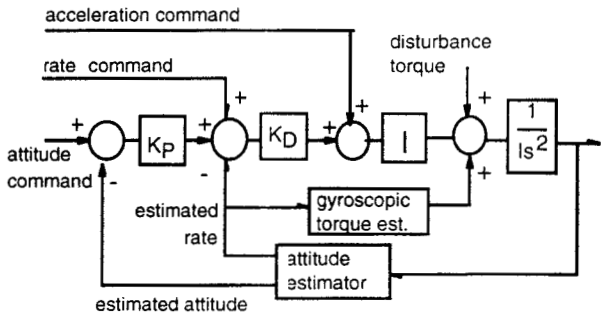

Fig. 4.4 A RWA controller design

In Fig. 4.4, K_P and K_D are the "proportional" and "derivative" gains of the RWA control loop. It can be shown that $K_P \cdot K_D = (2\pi \cdot BW)^2$ where BW is the bandwidth of the RWA controller. Since the RWA controller is a PD controller, in the presence of a persistent disturbance torque (T_D), the attitude controller error is non-zero, and is given by: $T_D/\{(2\pi \cdot BW)^2 \cdot I\}$, where I is the moment of inertia of the affected S/C's axis. Here, the controller error is defined as the difference between the commanded attitude vector and the ACS on-board estimation of the actual pointing vector. The magnitude of per-axis solar radiation torque imparted on the S/C is estimated to be: $T_D \approx 0.0005$ Nm (Lee, 1998). For a controller bandwidth of 0.1 Hz, and $I = I_{min} = 4000$ kg-m², the resultant attitude controller error could be estimated.

A mismatch in the gyroscopic terms used by the RWA controller can also cause a steady-state controller error. This error is: $(\Delta I/I)\cdot(2\pi\cdot BW)^{-2}\cdot(I_{max}-I_{min})\cdot\omega^2/I$. Here, $\Delta I/I$ is the percent knowledge error of the S/C's moment of inertia; I_{max} and I_{min} are the largest and smallest moments of inertia of the SIM spacecraft, respectively, and ω is the per-axis S/C rate. In this study, we use: $\Delta I/I$ = 10%, (I_{max}, I_{min}) = (36000,4000) kg-m², and $\omega \le 0.1$ °/s. An allocation of 3 sec is used in this study to account for attitude controller errors generated by these two disturbance sources.

To estimate the impact of the attitude estimator errors on the spacecraft pointing stability, via the RWA controller, we once again refer to Fig. 4.4. In order to capture the effect of the structural flexibility in our estimation, we replace the $1/Is^2$ term in Fig. 4.4 by a transfer function G(s) (where s is a Laplace variable) derived using the equations of motion of the spacecraft given in Section 4.5. In a quiescent state, the motion of the spacecraft θ is related to the spacecraft attitude error (n_θ) and rate error (n_ω) by the following expression:

$$\theta(s) = -[K_P/\Delta(s)]\cdot n_\theta - [K_D/\Delta(s)]\cdot n_\omega,$$

where $\Delta(s) = s + K_P + \{I\cdot K_D\cdot G(s)\}^{-1}$. We can then compute the power spectra of the spacecraft motion, $B^2(f)$, using these two transfer functions and the power spectral densities of the attitude and rate errors. Finally, the disturbance spectra are frequency-weighted by $W_d(C)$ (where $C = 2\pi fT$ and T = 10 msec) to determine the spacecraft pointing stability for 10-msec time windows.

4.7 RWA-induced structural vibrations

RWAs have three imperfections: dynamics imbalance, static imbalance, and axial runout. If the spin axis of the RWA is its Z axis, then the dynamic imbalance of the RWA is defined as: $I_D = \sqrt{\{I^2_{ZX} + I^2_{ZY}\}}$, where I_{ZX} and I_{ZY} denote the products of inertia's of the RWA in its X-Z and Y-Z planes, respectively. If the RWA is spinning at a rate of Ω_{rwa} rad/s, the dynamic imbalance generates a precessional disturbance torque with magnitude of $I_D\Omega^2_{rwa}$.

Instead of generating a disturbance torque, the static imbalance I_S of the RWA generates a precessional radial force. The static imbalance is the product of the RWA's mass and its eccentricity. If the RWA is spinning at a rate of Ω_{rwa} rad/s, the static imbalance generates a precessional radial disturbance force with magnitude of $I_S\Omega^2_{rwa}$. The resultant disturbance torque imparted on the S/C is $d\times I_S\cdot\Omega^2_{rwa}$, where d is a representative moment arm (cf. Fig. 4.5). Obviously, the closer we can place the RWAs with respect to the S/C's c.m., the smaller is the impact of this disturbance force on the angular motion of the spacecraft. The runouts (I_{RO}) of the RWAs produces an axial sinusoidal force that is also proportional to Ω^2_{rwa}.

Since the disturbance torque/force generated by the RWAs' imperfections are all proportional to Ω^2_{rwa}, one obvious way to limit the impact of these imperfections on the S/C pointing performance is to bound the RWAs' rpms at time when stringent pointing stability must be maintained. In this study, a bound of ±1000 rpm is used. A second way to limit the impact of these RWA imperfections is to mount the RWAs on vibration isolators. In this study, 15-Hz, 20% isolators are used.

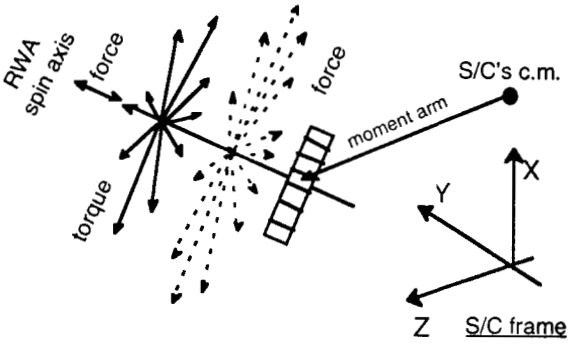

Fig. 4.5 RWA-induced disturbance forces and torques

The amplitude of the structural vibrations induced by three RWAs, each with three classes of disturbance torque's/forces could be estimated via simulation. Using the flexible S/C model described in Section 4.5, and assuming: $I_D = 9.1\cdot10^{-6}$ kg-m^2, $I_S = 3.6\cdot10^{-5}$ kg-m, $I_{RO} = 3.0\cdot10^{-5}$ kg-m, and d = 2 m, the 3σ amplitude of the RWA-induced vibrations is on the order of 0.6 mas.

To estimate the impact of these RWA-induced disturbance torque's on the spacecraft pointing stability, we first derive the transfer functions from these torque's to the spacecraft's angular displacement. The total disturbance spectra of the per-axis spacecraft motion, $B^2(f)$, are then computed using these transfer functions, and the power spectral densities of the RWAs' imperfections. The disturbance spectra are next frequency-weighted by $W_d(C)$ (where $C = 2\pi fT$, T = 10 msec) to determine the spacecraft pointing stability for 10-msec time windows. Finally, the computed pointing stability is increased by a factor of 1.5 to account for effects due to the unmodelled high-frequency structural modes of the SIM precision structure.

4.8 S/C-solar array control interaction

With reference to Fig. 1.1, the solar array/sun shield is attached to the spacecraft basebody via a solar array boom. The relative orientation of the boom with respect to the basebody is to be controlled via a 2-dof solar array drive mechanism (SADM). The solar array is to be controlled to within 0.5-1° of the sunline vector at all time in order to shield several basebody-mounted instruments from direct solar radiation. This arrangement enables the thermal control of these instruments to within very tight temperature bounds.

In order to point the science interferometer at a new target star, the spacecraft ACS must first compute two solar array articulation angles using the inertial position knowledge of both the target star and the Sun. Next, these computed angles are sent as commands to a two-axis solar array control loop. Once the new

spacecraft orientation is achieved, the SA pointing loops are "disabled" (angle commands to stepper motors are set to zero), and the SA boom is being held in position passively by both friction and the stepper motor cogging torques (after they have been amplified by the harmonic drive). With no control torque from the SA control loops, the spacecraft basebody will not experience any "reaction" torque (from the SA control loops) which might negatively impact the pointing stability of the spacecraft.

4.9 Thermal flutter

Thermal flutter on a spacecraft is most pronounced when there is a rapid heating rate change on one or more spacecraft structural members (e.g., its solar array or a flexible boom). Undesirable scenarios include spacecraft that makes frequent orbital eclipse transitions (Foster, et al, 1995), and for a spin-stabilized spacecraft with a long flexible boom. None of these scenarios is applicable to the SIM spacecraft which is a three-axis stabilized spacecraft in a Earth-trailing orbit. Nevertheless, an upper bound on the power spectral density of the SA-induced disturbance torque is used in this study to limit the impact of thermal flutter on the pointing stability of the spacecraft basebody. See Fig. 4.6.

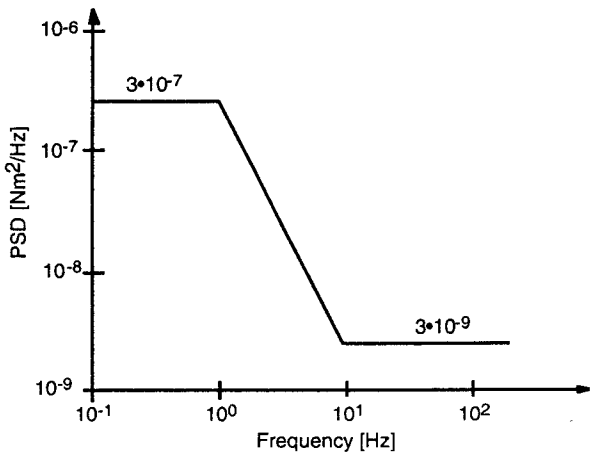

Fig. 4.6 Upper bound of PSD of solar array-induced disturbance torque

4.10 S/C-interferometers control interaction

For SIM to successfully perform an astrometric measurement, its Real-Time Control (RTC) subsystem must accomplish two tasks: (1) the angle pointing control loop must be able to initially acquire, then track (via fast steering mirrors) the target stars, and (2) the fringe tracker control system must acquire a stellar fringe (via stepper motors, VC, and PZT actuators), then stabilize the stellar fringe position. Disturbance torque's generated by these RTC control systems must be bounded in order to limit their impact on the spacecraft pointing stability. An upper bound on the power spectral density of RTC-induced disturbance torque is depicted in Fig. 4.7.

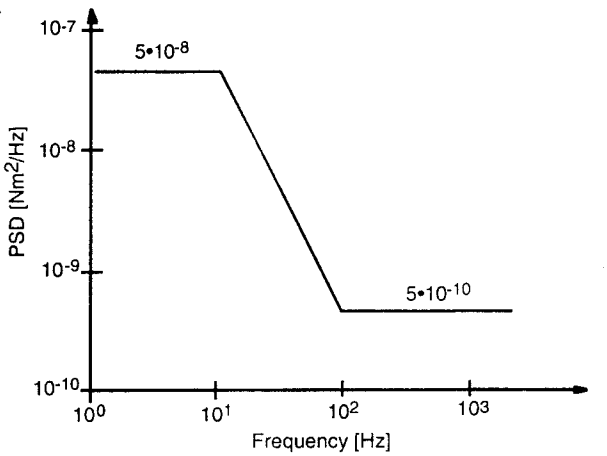

Fig. 4.7 Bound on PSD of RTC-induced disturbance torque

5. Preliminary error budgets

The "sizes" of various error contributors to the spacecraft pointing knowledge, control, and stability could be estimated using approaches described in Section 4. In Table 5.1, these component errors are root sum squared (RSS'ed) together to obtain the 3σ capability of the spacecraft pointing knowledge. The estimated overall capabilities are 7.3 and 66.8 sec about the S/C's X and Z, and Y axes, respectively. They are better than the requirements with good margin.

Table 5.1 Pointing Knowledge Error Budget

Error sources	3σ per axis [sec]	
	X and Z axes	Y axis
attitude determination error	0.18	1.5
SRU bias	3.1	47
residual calibration error	3.2	47.1
SRU thermal mechanical instability	4	4
SIM frame thermal mechanical instability	0*	0*
slew-induced structural vibration	<0.001	<0.001
RWA-induced structural vibration	<0.001	<0.001
SIM structural thermal distortion	1	1
target command error	4	4
pointing knowledge capability	7.3	66.8
pointing knowledge requirement	20	120

Table 5.2 is an error budget for the spacecraft control requirements. Again, we RSS together various component errors (other than that of the RWA controller error). The overall spacecraft pointing capabilities are determined by adding algebraically the RSS result and the RWA controller error. The estimated overall capabilities are 10.3 and 69.8 sec about the S/C's X and Z, and Y axes, respectively. Again, we met the requirements with good margin.

Table 5.2 Pointing Control Error Budget

Error sources	3σ per axis [sec]	
	X and Z axes	Y axis
attitude determination error	0.18	1.5
SRU bias	3.1	47
residual calibration error	3.2	47.1
SRU thermal mechanical instability	4	4
SIM frame thermal mechanical instability	0*	0*
slew-induced structural vibration	<0.001	<0.001
RWA-induced structural vibration	<0.001	<0.001
SIM structural thermal distortion	1	1
target command error	4	4
root-sum-squares	7.3	66.8
RWA controller error	3	3
pointing control capability	10.3	69.8
pointing control requirement	30	120

Table 5.3 is an error budget for the spacecraft pointing stability requirement. Again, the component errors which are all 1σ values are RSSed together to estimate the 1σ capability of the spacecraft pointing stability. The estimated overall capability is 0.39 mas which just meets the requirement. There isn't a good margin between the requirement and capability.

6. Conclusions

Preliminary error budgets for the pointing knowledge, control, and stability of the SIM spacecraft are constructed using the specifications of commercial off-the-shelf attitude determination sensors, attitude control actuators, and other spacecraft capabilities that had been demonstrated in past missions. Results obtained indicate that we can meet all the presently known spacecraft pointing requirements. Among all the spacecraft pointing requirements considered, the pointing stability requirement is the most challenging.

A large number of "children" requirements are generated from this study. Top on the list, as expected, are specifications on attitude determination sensors and attitude control actuators. Other requirements include the minimum settling time after a rest-to-rest spacecraft slew, frequency and damping of the solar array boom, and others. Since the SIM spacecraft design is expected to evolve with time, pointing requirements stated in this study are likely to change with it. Hence, error budgets constructed here must be revised to reflect the changing spacecraft design. Also, the currently identified pointing requirements might have to be modified as a result of changes made to the SIM spacecraft and instrument designs, and new pointing requirements added. Results given here represent only the first step.

Table 5.3 Pointing Stability Error Budget

Error Sources	1σ per axis (X and Z axis) [mas]
S/C attitude determination and control system:	
• Control error:	
RWA command resolution	0.01
Controller timing jitter and delay	0.05
RWA speed reversals	0*
• Attitude determination:	
IRU and SRU noise	0.27
Disturbances:	
• SA/SS drive mechanisms†	0*
• HGA drive mechanisms	0*
• RWA-induced vibrations	0.26
• Tape recorders (playback and rewind)†	0*
• interferometer control systems: angle and fringe trackings	0.041
Thermal-mechanical vibrations:	
• slew-induced vibrations	0.012
• solar array thermal flutter	0.1
• precision structure thermal instability	0*
per-axis capabilities	0.39
per-axis requirement	0.4

†Via careful sequence planning, these events are to be inhibited at times when tight pointing stability requirement must be met.

7. References

Aaron, K., 1998, "SIM Rainbird Configuration," Internal JPL Presentation Package.

Aaron, K. and Mateer, W., 1998, "Inertia Properties of the SIM Spacecraft and Its Solar Array," Internal JPL Presentation Package.

Chu, C.C., 1998, "TBD", Internal JPL Presentation Package.

Foster, C.L., Tinker, M.L., Nurre, G.S., and Till, W.A., 1995, "Solar-Array-Induced Disturbance of the Hubble

Space Telescope Pointing System," Journal of Spacecraft and Rockets, Vol. 32, No. 4.

Laskin, R., 1998, "Dynamics and Control Requirements Flowdown," PISRR Presentation Package (TBD).

Lee, A., 1997, "Cassini Functional Requirements Document: System Accuracy Requirements and Predicted Capabilities," CAS-3-170.

Lee, A., 1998, "AACS Issues related to SIM Reaction Wheel Unloading" JPL Internal memorandum 3412-98-36, April 7, 1998.

Lucke, R.L., Sirlin, S.W., and San Martin, A.M., 1992, "New Definitions of Pointing Stability: AC and DC Effects," The Journal of Astronautical Sciences, Vol. 40, No. 4, pp. 557-576.

Macala, G., 1994, "Cassini Attitude Control by Reaction Wheels," JPL engineering memorandum 345-006.

Rayman, M. and Shao, M., 1992, "A Mission and System Design Option for the Orbiting Stellar Interferometer," IAF-92-0527, 43rd Congress of the International Astronautical Federation, Washington, D.C.

Yu, J., 1998, "SIM Instrument Requirements and Error Budgets" PISRR Presentation Package (TBD).

8. Acronyms

AACS	Attitude and Articulation Control Subsystem
ACS	Attitude Control Subsystem
ATE	Attitude Estimator
BW	Bandwidth (of a controller)
c.m.	center of mass
c.p.	center of pressure
COTS	Commercial-Off-The-Shelf
dof	degree of freedom
FOR	Field of Regard
FOV	Field of View
HGA	High Gain Antenna
IRU	Inertial Reference Unit
LOS	Line Of Sight
mas	milli-arc-second
min	arc-minute
MOI	Moment of Inertia
NEA	Noise Equivalent Angle
PD	Proportional+Derivative (controller)
PISRR	Preliminary Instrument System Requirement Review
ppm	part per million
PSD	Power Spectral Density
PSF	Point Spread Function
PSS	Precision Structure Subsystem
PZT	Piezo-electric (actuator)
RMS	Root-Mean-Squares
RSS	Root-Sum-Squares
RTC	Real-time Control Subsystem
RWA	Reaction Wheel Assembly
SADM	Solar Array Drive Mechanism
SA/SS	Solar Array/Sun Shield
S/C	Spacecraft
sec	arc-second
SIM	Space Interferometry Mission
SRU	Stellar Reference Unit (star tracker)
TBD	To Be Determined
VC	Voice Coil

9. Acknowledgments

The research described in this paper was carried out by the Jet Propulsion Laboratory, California Institute of Technology, and was sponsored by the National Aeronautics and Space Administration. The authors wish to thank K. Aaron, D. Bayard, R. Blue, G. M. Brown, C. Chu, P. Kobele, R. Laskin, G. Macala, J. Reimer, M. San Martin, L. Sievers, and G. Tsuyuki, their colleagues at JPL, for many helpful discussions.

10. About the authors

Allan Lee is a systems engineer at the Avionics Systems Engineering section of Jet Propulsion Laboratory. In 1990-1997, he worked on the definition, design, test, and launch of the Cassini spacecraft. Systems engineering tasks he performed include system accuracy requirement definitions and capability predictions, fault protection design of the attitude and articulation control subsystem, flight software testing, command and telemetry dictionaries, and others. He also worked on various spacecraft control-related R&D topics: model reduction methodologies for articulated, multi-flexible body space structures (for example, the Galileo

spacecraft), development of neural networks-based spacecraft guidance algorithms, and others. Dr. Lee has earned a Ph.D. in Aeronautics and Astronautics from Stanford University. In 1985-89, he was a senior staff research engineer with the General Motors Research and Development Laboratories. In addition to tasks that are related to the Space Interferometry Mission, he is currently supporting the mission operations of the Cassini spacecraft as well as the development of a variable dynamic testbed vehicle. The latter is to be used by researchers at the National Highway Traffic Safety Administration (NHTSA) in studies that are related to automobile dynamics and control, pre-accident driver-vehicle interactions, and others.

Jeffrey Yu (TBD).

Peter Kahn (TBD).

Richard Stoller (TBD).